

DIFFRACTION OF RESONANCE γ RAYS BY NUCLEI AND ELECTRONS IN TIN SINGLE CRYSTALS

V. K. VOĬTOVETSKIĬ, I. L. KORSUNSKIĬ, A. I. NOVIKOV and Yu. F. PAZHIN

Submitted December 15, 1967

Zh. Eksp. Teor. Fiz. 54, 1361–1373 (May, 1968)

Diffraction of resonance γ rays in Sn^{119} single crystals is investigated experimentally. The nature of the scattering spectra at the Bragg angle as functions of the relation between the nuclear and electron scattering amplitudes is analyzed. Diffraction of resonance-scattered radiation by Sn^{119} nuclei and interference of resonance-scattered radiation with the radiation scattered by the electrons are distinctly observable. The experimental data agree with the calculations for crystals with a mosaic structure.

INTRODUCTION

THE Mössbauer effect makes it possible to confirm experimentally the coherence of radiation scattered by resonant centers^[1-4], in the particularly interesting case of resonant scattering by nuclei having low-lying levels with lifetimes that are tremendous on a nuclear scale, namely $\sim 10^{-8}$ – 10^{-7} sec.

Recently Afanas'ev and Kagan^[5] developed a consistent dynamic theory of the resonant interaction between particles and radiation from a regular system of nuclei. The theory predicts a number of new results; in particular, in an ideal crystal the inelastic reaction channels can be suppressed under certain conditions, and the material ceases to be absorbing and becomes transparent or partially transparent. Other predicted effects^[6], for example the formation of a collective nuclear level, can be observed also in crystals with not so perfect a structure.

The theory is based on the assumption that the radiation resonantly scattered by the nuclei is coherent, and the confirmation of this assumption should naturally also be the first stage in the realization of the program of experimental investigations of the resonant interaction of radiation with a regular system of nuclei. The coherence of a resonantly scattered wave with the primary beam can be established by means of the interference between the radiation resonantly scattered by the nucleus and the radiation scattered by the electrons. The coherence of waves scattered by individual nuclei can be directly confirmed by observing the diffraction of the gamma radiation resonantly scattered by nuclei in a single crystal¹⁾.

As is customary in experiments aimed at investigating absorption and scattering without recoil, the nuclear scattering can be revealed by the dependence of the intensity of the scattered radiation on the relative velocity of the source and the scatterer—the scattering spectrum. If the amplitudes of the Rayleigh electron and resonant nuclear scatterings are comparable in this case, then the spectrum of scattering at the Bragg angle not only contains the electronic nuclear components, but is determined to a considerable degree by the interfer-

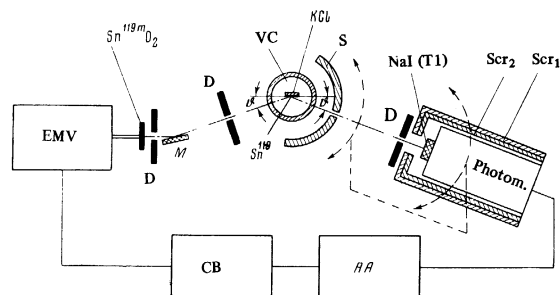


FIG. 1. Diagram of experimental setup: M — monochromator, D — diaphragms, VC — vacuum chamber of cryostat, S — iron shield, Scr₁ — lead screen, Scr₂ — steel screen, EMV — electromagnetic vibrator, CB — control block, AA — pulse-height analyzer.

ence between the nuclear and electron scattering, thus making it possible to combine the two experiments.

Experiments aimed at confirming the coherence of resonantly scattered radiation can be performed with both ideal and mosaic crystals, but the character of the scattering spectrum for crystals of different structure will differ appreciably, and the form of the scattering spectrum may even serve as an effective criterion for the degree of perfection of the crystal structure. This difference is most strongly observed for thick crystals, and becomes smoothed out with decreasing thickness, corresponding to a transition to the kinematic approximation.

Black, Moon, et al. performed experiments aimed at observing the interference between the resonant and Rayleigh scattering in poly-crystalline samples of iron^[8] and single crystals of iron of natural isotopic composition^[9]. In these experiments, the spectra of scattering at the Bragg angle revealed a small asymmetry of the peak of the nuclear scattering^[8], connected with the interference effect, as well as a dip due to absorption^[9].

We investigated experimentally the diffraction of resonant gamma radiation in single crystals of tin containing 80% Sn^{119} . The dependence of the intensity of the radiation scattered at the Bragg angle on the velocity of the source relative to the scatterer was investigated in single crystals with varying thicknesses at temperatures 293 and 110–120°K in three orders of reflection.

¹⁾Observation of diffraction of γ radiation resonantly scattered by Fe^{57} nuclei was reported in [7].

Resonant scattering by the Sn^{119} and interference between the resonantly scattered radiation and the radiation scattered by the electrons were observed in the diffraction peaks. The interference was particularly clearly pronounced when the ratio of the nuclear scattering amplitude (at resonance) to the electronic amplitude was $\sim 3-4$; if this ratio is ≥ 6 , then the diffraction of the radiation resonantly scattered by the nuclei begins to predominate in the scattering spectrum. The results of the experiments were compared with the theory of Bragg scattering by resonant systems^[10].

2. EXPERIMENTAL PROCEDURE

We used in the experimental setup (Fig. 1) a two-crystal spectrometer based on a modernized type GUR-4 goniometer, as well as a constant-velocity Mössbauer spectrometer (of the discrete type). The reflecting-crystal positions were (1, -1). The monochromator was an LiF single crystal. The scattered radiation was registered by a scintillation counter with a single-channel pulse-height analyzer. The spectrometer was adjusted with the aid of an intense (~ 1 Curie) $\text{In}^{114\text{m}}$ x-radiation source with energy 24.1 keV, simulating the weaker γ radiation of $\text{Sn}^{119\text{m}}$ (23.8 keV).

The source of the resonant γ radiation was a layer of $\text{Sn}^{119\text{m}}\text{O}_2$ with area 1×10 mm. The sources were prepared by irradiating metallic tin (Sn^{118} content 95%) in the neutron beam of the high-power SM reactor and had an intensity 8–16 mCi/cm². The irradiated tin was transformed after special purification²⁾ into the dioxide by roasting. The powdered tin dioxide was precipitated from an alcohol solution (with a small addition of BF resin) onto an aluminum plate.

The intensity of the resonant scattering, particularly in the third reflection order, was small, so that the reduction of the counter background to the lowest possible value was very important. The counter employed in NaI(Tl) crystal (thickness 1 mm, area 6×12 mm) with a diffuse reflector of magnesium oxide, and an FEU-74 photomultiplier (with multislit photocathode) having high sensitivity and low noise level. The resolution of the counter for the photopeak of the γ radiation with energy 24 keV was approximately 25%. The width of the pulse-height analyzer channel corresponded to complete registration of the 23.8-keV radiation.

Intense x radiation with energy 25.1 keV, accompanying the conversion from the upper level of $\text{Sn}^{119\text{m}}$, was separated with a monochromator and was cut off almost completely by a diaphragm placed behind the monochromator. The scintillation counter was screened with a 3-mm layer of steel and a 2-mm layer of lead, and protected against the radiation scattered by the parts of the apparatus by means of an iron layer 5 cm thick. The intrinsic background of the counter was 0.5 count/min in the registered range of amplitudes.

The single crystals of Sn^{119} used in the experiments, with thickness 2–16 μ , were obtained by an epitaxial method. The films of tin were grown on KCl single crystals 0.5–2 mm thick and with area 20×20 mm. The surfaces of the crystal were parallel to the (020)

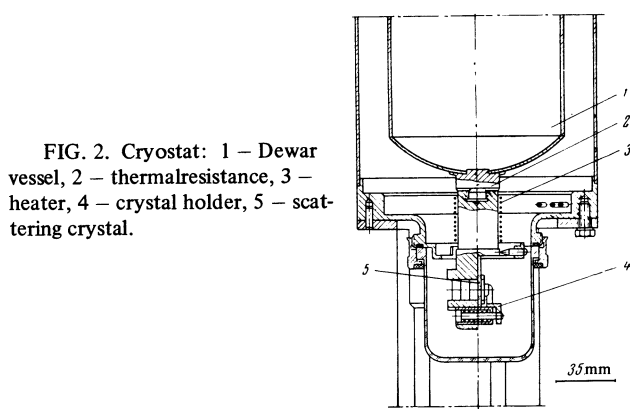


FIG. 2. Cryostat: 1 – Dewar vessel, 2 – thermalresistance, 3 – heater, 4 – crystal holder, 5 – scattering crystal.

crystallographic plane. The known methods of determining the thickness were insufficiently reliable for the measurement of the thicknesses of the obtained films. Therefore the layer thickness determined from the scattering of the x-rays and by usual weighing was monitored also by weighing the film in a liquid compensating for the weight of the $\text{KCl}^{[11]}$. This method made it possible to measure the thickness of the tin single crystals with accuracy 5–10%. The quality of the crystals was verified against the diffraction of the characteristics x-radiation of molybdenum (19.6-keV K_{β} line). In the measurements made at low temperatures, we used a nitrogen cryostat with adjustable temperature, the construction of which is shown in Fig. 2. The scattering crystal was mounted on a bulky copper holder and was in an evacuated chamber of Plexiglas 0.5 mm thick, which was practically transparent to the γ radiation of the $\text{Sn}^{119\text{m}}$. The temperature of the crystal was determined with the aid of a chromel-copel thermocouple.

In measurements of the dependence of the intensity of the scattered (transmitted) radiation on the relative source and scatter (absorber) velocity, the source was set in motion by means of an electromagnetic vibrator. The source velocity range was from -8 to $+11.5$ mm/sec. Each experimental curve contains 36 points. The independence of the efficiency of registering the scattered radiation of the position and velocity of the source was verified beforehand by scattering x-rays of energy 25.1 keV from the tin single crystal.

To calibrate the Mössbauer spectrometer and to determine the width of the emission line, we plotted the spectra of recoilless resonant absorption by single crystal Sn^{119} and by polycrystalline foil. One such spectrum is shown in Fig. 3³⁾. The accuracy with which the velocity scale of the Mössbauer spectrometer was calibrated was 1%. The stability of the source velocity was monitored regularly during the course of the measurements, and amounted to 2%.

The instability of the pulse counting rate at each point of the scattering or absorption spectrum did not exceed 1%.

3. MEASUREMENT RESULTS

Figure 4 shows the diffraction peak obtained in the scattering of 23.8-keV γ radiation by an Sn^{119} single-

²⁾The authors use the opportunity to thank L. V. Chistyakov for purifying the irradiated tin.

³⁾The chemical shift for tin is 2.55 mm/sec, corresponding to an energy 20.5×10^{-8} ev.

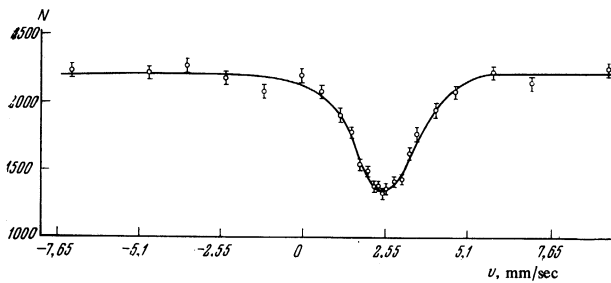


FIG. 3. Spectrum of recoilless resonant absorption in single crystal Sn^{119} 16 μ thick at $T = 120^\circ\text{K}$. N – total number of counts of scintillation counter.

crystal film 5 μ thick. In the position corresponding to the maximum of the diffraction peak, we measured the dependence of the intensity of the scattered radiation on the velocity of the source relative to the scatterer. The character of the scattering spectrum was determined by the relation between the amplitude f_{nuc} of scattering by the nucleus and the amplitude f_e of scattering by the electrons. The main purpose of the experiment was to observe directly in the scattering spectrum the interference and diffraction of the radiation resonantly scattered by the nuclei. To this end it was necessary to carry out the measurements at a large value of the ratio f_{nuc}/f_e .

In the first reflection order, the Bragg angle for the (020) plane of the single crystal of tin is $5^\circ 7'$. This angle corresponds to the large value $f_e = 1.15 \times 10^{-11}$ cm; at room temperature $f_{\text{nuc}}^r/f_e = 0.45$, where f_{nuc}^r is the amplitude of scattering by the nucleus at resonant energy. To determine the dependence of the intensity of the scattered radiation on the source velocity at large values of f_{nuc}^r/f_e , the measurements were performed at a temperature $T = 110$ – 120°K (a reduction of the temperature increases the Mössbauer factor, and consequently increases f_{nuc}^r in the first, second, and third, reflection orders (f_e decreases with increasing reflection order, owing to the change in the atomic factor). The increase of the reflection order is more effective than the further reduction of the temperature. Lowering the temperature, accompanied by a simultaneous increase of f_{nuc}^r , leads simultaneously to an intensification of the resonant absorption, thus deepening the dip in the scattering spectrum in the resonance region, thereby masking the nuclear scattering.

The experimentally obtained dependence of the intensity of the $\text{Sn}^{119\text{m}}$ γ -radiation scattered by the tin single crystal at the Bragg angle on the relative velocity of the source and the scatterer v is shown in Fig. 5. These

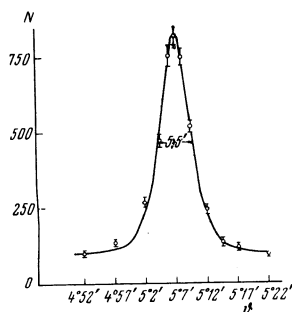


FIG. 4. Angular dependence of the intensity of 23.8-keV γ radiation scattered by single-crystal tin near the Bragg angle in first order of reflection. The Sn film thickness is 5 μ , the reflection plane is (020). N – total number of counts of scintillation counter.

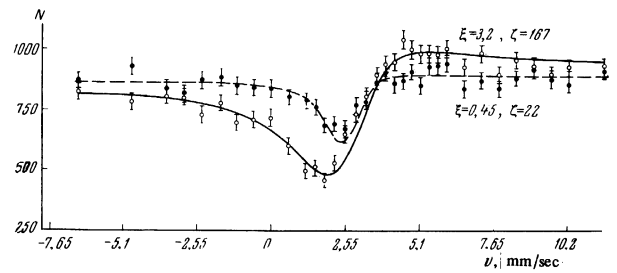


FIG. 5. Spectrum of 23.8-keV γ radiation scattered by single-crystal Sn^{119} at the Bragg angle in first order of reflection: \bullet – $T = 293^\circ\text{K}$, \circ – $T = 110^\circ\text{K}$ ($l = 3 \mu$). N – number of counts of scintillation counter without background. The curves were calculated under the assumption that the crystal has a mosaic structure. (Here and in the following figures $\xi \equiv f_{\text{nuc}}^r/f_e$ and $\zeta \equiv \mu_{\text{nuc}}^r/\mu_e$).

measurements were made in first order of reflection at temperatures 293 and 110°K . The thickness l of the tin single crystal was $l = 3 \mu$. The background, ranging from 18 to 35% of the total intensity of the registered radiation, was subtracted beforehand. To determine the background, the crystal and the detector were shifted 2° from the position corresponding to the Bragg angle. The statistical accuracy at each point of the curve (with allowance for the errors introduced by the background) was 4–6%. The background from the inelastic coherent scattering, estimated to be within the limits of the statistical accuracy of the measurements, was not taken into account.

When the temperature is decreased to 110°K , the ratio $\xi \equiv f_{\text{nuc}}^r/f_e$ changes by approximately 7 times. As seen from the experimental curves, the interference between the resonant nuclear and electron scattering, which becomes manifest at room temperature in an asymmetry of the dip of the resonant absorption, leads at 110°K to a sharp increase of the intensity of one side of the resonant velocity and to a decrease on the other, determining to a considerable degree the entire character of the scattering spectrum. The resonant absorption becomes stronger (the ratio of the coefficient of nuclear absorption at resonance to the coefficient of the electron absorption $\zeta \equiv \mu_{\text{nuc}}^r/\mu_e$ increases by ~ 7.5 times), but the minimum of the curve shifts to the left, owing to the influence of the interference.

The ratio f_{nuc}^r/f_e increases even more on going to reflection in the second and third orders. Figure 6 shows the same dependence as Fig. 5, but for reflection in the first (I), second (II), and third (III) orders for single crystals of equal thickness at temperatures 110– 120°K . They also show the intensity of the resonant radiation relative to the intensity of the incident radiation. The plot is shown separately for the reflection in second and third orders in an enlarged scale. The background in these experiments were 7–40% (I), 17–50% (II), and 40–80% (III). The statistical measurement accuracy at each point was 2–6% (I), 3–7% (II), and 4–12% (III). The total intensity of the scattered radiation decreased rapidly with increasing order of reflection.

Comparison of the experimental curves on Fig. 6 shows that on going to reflection in higher orders the role of the interference increases appreciably, and that of the nuclear component of scattering increases to an

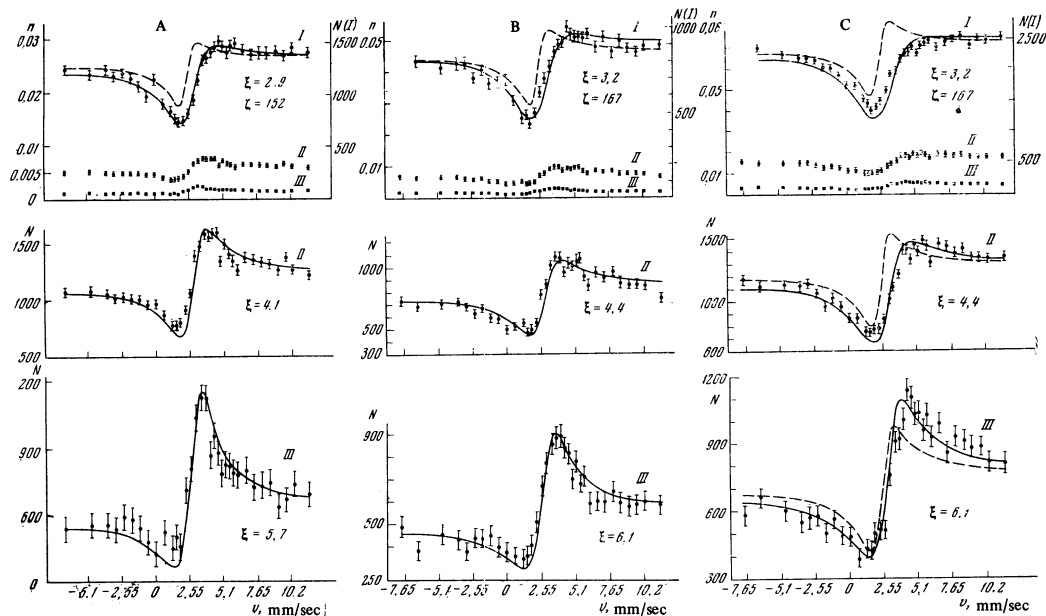


FIG. 6. Spectra of 23.8-keV γ radiation scattered by single-crystal Sn^{119} at the Bragg angle in three orders of reflection (I – first order, II – second order, III – third order) in the following cases: A) $l = 2 \mu$, $T = 120^\circ \text{K}$; B) $l = 3 \mu$, $T = 110^\circ \text{K}$; C) $l = 5 \mu$, $T = 110^\circ \text{K}$ (n – intensity of scattered radiation relative to the intensity of the incident radiation, N – number of counts of scintillation counter without the background). The solid curves were calculated for crystals with mosaic structure, the dashed curves for ideal crystals.

even greater degree; the latter is manifest in the form of a narrow peak in the resonance region. The influence of the interference displaces the peak due to the nuclear scattering to the right. The same figures, and also Fig. 7, show the theoretical curves obtained assuming perfect and mosaic crystal structures. For crystals with perfect structure, a rigorous calculation was performed on the basis of the dynamic theory of the interaction of the resonant gamma radiation with nuclei and electrons in the single crystal^[10]. In the case of a mosaic crystal, it was assumed that the secondary extinction can be neglected. In the calculations with the M-20 electronic computer, we used the values of the atomic factors, conversion coefficient, and Mössbauer coefficients from^[12,13] 4). The experimentally obtained source emission line width turned out to be, with allowance for the quadrupole splitting, close to the natural width. The theoretical curves were normalized by least squares to the experimental points in the region of the maximum values of the absolute velocity.

As noted earlier, the theoretical γ -ray resonant-scattering spectra for ideal and mosaic crystals differ most strongly when the crystals are thick (an increase in the order of the reflection decreases the effective thickness of the crystal). The experimental curves are close to the calculated ones for mosaic single crystals, while the theoretical relations for ideal crystals deviate considerably from experiment.

The mosaic character of the structure of single-crystal epitaxial films is evidenced also by an analysis of the experimental half-width of the diffraction peaks and the relative intensity of the radiation scattered in different orders of reflection. The half-width of the diffraction peak for tin is $5.5'$ (Fig. 4). The half-width

Table I. Relative intensities of 23.8-keV γ radiation scattered by single crystals of tin at the Bragg angle*

Order of reflection	Experiment	Calculation	
		Mosaic crystal	Ideal crystal
$l = 2 \mu, T = 120^\circ \text{K}$			
I	21	31.5	8.4
II	4.4	4.56	3
III	1	1	1
$l = 5 \mu, T = 110^\circ \text{K}$			
I	61	61	8
II	13	10.5	3
III	2.9	2.3	1.35

*The angular divergence of the beam is $4'$. The experimental and calculated values of the intensity of the scattered γ radiation in reflection in the third order by a crystal of 2μ thickness is taken as unity.

of the peak is determined by the mosaic structure of the crystal and by the divergence of the beam. The angular divergence of the recorded part of the beam scattered by the monochromator (transmitted by the diaphragm) amounted to $4'$ in these measurements. In measurements with $\text{Mo K}\beta$ x-radiation, when the divergence of the beam did not exceed $40''$, the half-width of the peak at the Bragg angle was $2.5' - 9'$ for the different crystals, thus clearly proving the mosaic structure of the crystals. (The half-width of the diffraction peak, measured with the same x-ray beam in crystals of tin $0.2 - 0.6$ mm thick and grown on an oriented primer, was smaller than $1'$. Such crystals have a more perfect structure, with violations of apparently only local character, since we succeeded in observing the Borrmann effect in these crystals^[14].)

4) The theoretical curves were calculated by I. P. Perstnev.

Table II. Relative intensities of Mo K_{β} x-radiation (19.6 keV) scattered by tin single crystals at the Bragg angle*

Order of reflection	Experiment		Calculation	
	Epitaxial single-crystal film, $l = 5 \mu$	Single crystal, $l = 0.4 \text{ mm}$.	Mosaic crystal	Ideal crystal
I	28	6.5	36.7	7.2
II	5.9	2.4	5.4	2.5
III	1	1	1	1

*Angular beam divergence $< 40''$. The experimental and calculated values of the intensity of the scattered x-radiation reflected in third order are taken equal to unity.

Table I compares the experimental relative intensities of the radiation of $\text{Sn}^{119\text{m}}$, scattered by single crystals of tin in the first, second, and third orders of reflection, at temperatures 110–120°K, and the calculated values of these quantities for ideal and mosaic crystals of tin. The experimental data are close to those calculated for crystals with mosaic structure.

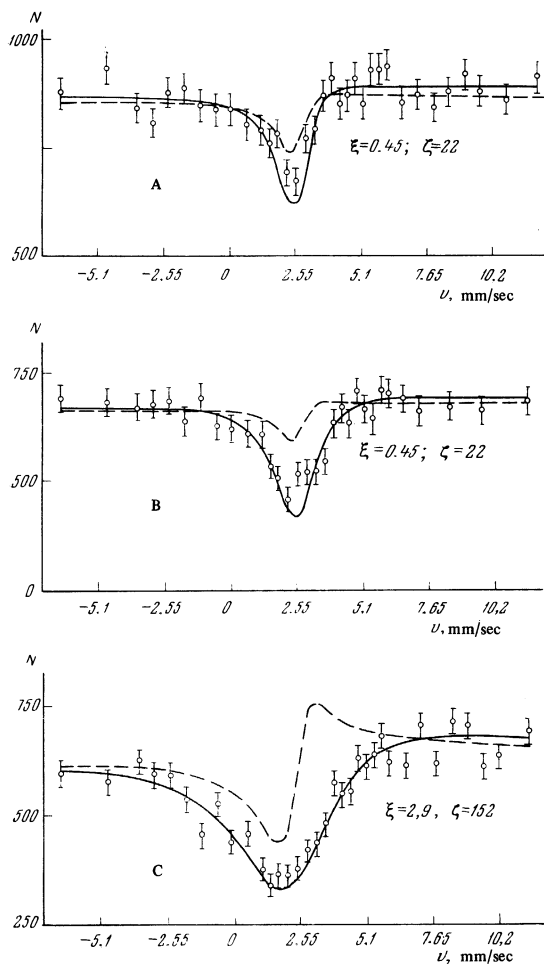


FIG. 7. Spectra of 23.8-keV γ radiation scattered by single-crystal Sn^{119} at the Bragg angle in the first order of reflection. A) $l = 3 \mu$, $T = 293^\circ\text{K}$, B) $l = 16 \mu$, $T = 293^\circ\text{K}$; B) $l = 16 \mu$, $T = 120^\circ\text{K}$. The solid curves were calculated for crystals of mosaic structure, the dashed curves dashed for ideal crystals (N – number of counts without background).

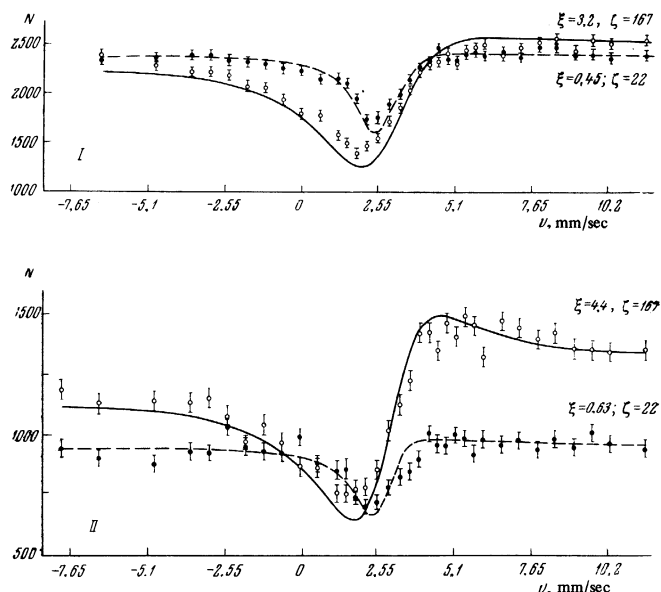


FIG. 8. Spectra of 23.8-keV γ radiation scattered by single-crystal Sn^{119} , $l = 5 \mu$, at the Bragg angle in the first (I) and second (II) orders of reflection at \bullet – $T = 293^\circ\text{K}$ and \circ – $T = 110^\circ\text{K}$. (N – number of count of scintillation counter without background.) The solid curve was calculated for a crystal with mosaic structure at $T = 110^\circ\text{K}$, and the dashed curve at $T = 293^\circ\text{K}$.

Table II shows the measured and calculated values of the same quantities in scattering of Mo K_{β} x-radiation by single crystals of tin. The measurements were made with a two-crystal spectrometer with a beam divergence smaller than $40''$. The same table lists the data obtained for more perfect single crystals of tin (judging from the width of the diffraction peaks and from the observation of anomalous transmission) of thickness 0.4 mm. It follows from Table II that the experimental data for thin epitaxial layers agree with the calculated ones for mosaic crystals, while the experimental results for single crystals 0.4 mm thick are close to the calculated ones for ideal crystals.

Figure 8, II shows the scattering spectrum at temperatures 293 and 110°K, for a tin single crystal 5 μ thick in the second order of reflection. The intensity of the scattered radiation, unlike the first-order reflection (Fig. 8, I), is somewhat higher at low temperature, since the sensitivity of the structure factor to the temperature increases in second order. At 110°K, the spectrum has the form characteristic for interference of the scattering by nuclei and electrons.

The influence of the lowering of the temperature and of the transition to higher orders of reflection is seen particularly clearly in Fig. 9, which shows the dependence of the intensity of the scattered radiation on the relative velocity of the source and scatterer at $T = 293^\circ\text{K}$ in first order and $T = 110$ – 120°K in three orders of reflection. These plots are normalized to a velocity -6.7 mm/sec . (We normalized the calculated curves for crystals with mosaic structure, each curve being normalized to all the experimental points by least squares.)

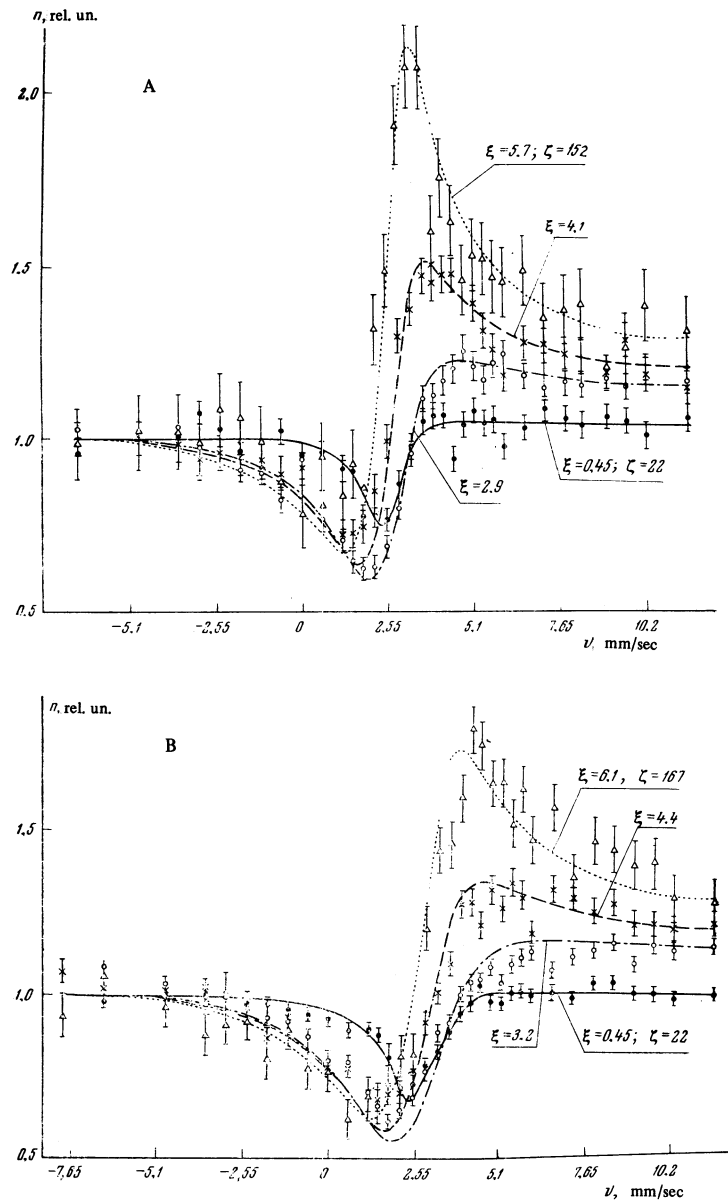


FIG. 9. Normalized spectra of 23.8-keV γ radiation scattered by single-crystal Sn^{119} at the Bragg angle at $T = 293^\circ\text{K}$ in first order of reflection (\bullet) and $T = 110\text{--}120^\circ\text{K}$ in first (\circ), second (\times), and third (Δ) orders of reflection. A) $l = 2 \mu$, $T = 293^\circ$ and 120°K ; B) $l = 5 \mu$, $T = 293$ and 110°K . The curves were calculated under the assumption that the crystal has a mosaic structure.

Figure 10 shows the influence of the thickness of the crystal on the character of the scattering spectra in reflection in the first and third orders. The experimental plots are normalized as in Fig. 9. With increasing crystal thickness, the curves become less steep, and the larger role of absorption causes the role of the nuclear component of the scattering to decrease and the maximum to shift to the right. (This should not take place for an ideal crystal.)

Variation of the temperature and of the order of the reflection in our experiments have made it possible to modify appreciably the character of the scattering

spectrum, separating the individual components distinctly. Observation of the diffraction in resonant scattering by nuclei and interference of the Rayleigh and resonant scattering confirms the coherence of the radiation resonantly scattered by the nuclei, and demonstrates the feasibility of experimentally observing effects connected with collective interaction between resonant radiation and irregular system of nuclei.

The authors are grateful to A. P. Aleksandrov for interest in the work, Yu. M. Kagan, A. M. Afanas'ev, and I. P. Perstnev for a discussion of the results, É. F. Chaikovskii and N. M. Loboda for preparing the

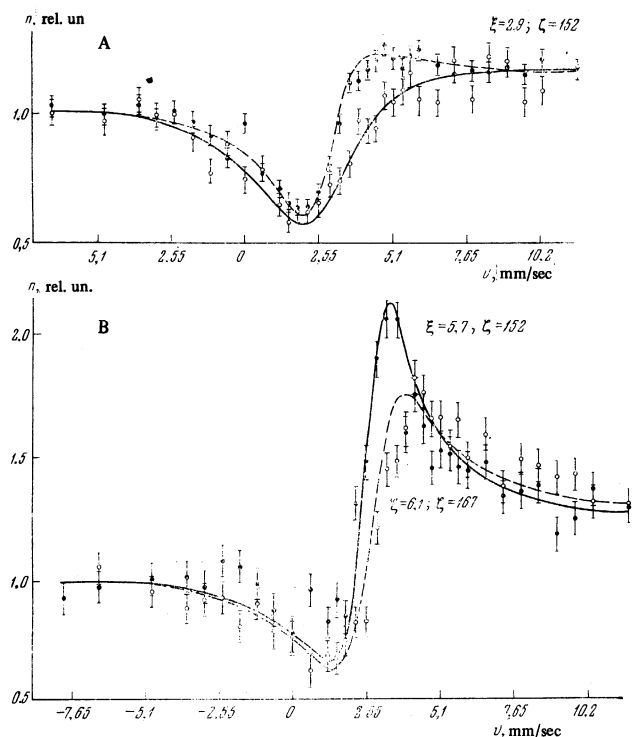


FIG. 10. Normalized spectra of 23.8-keV γ radiation scattered by single-crystal Sn^{119} at the Bragg angle: A — crystal thickness 2μ (\bullet) and 16μ (\circ), first order of reflection, $T = 120^\circ\text{K}$; B — crystal thickness 2μ , $T = 120^\circ\text{K}$ (\bullet) and crystal thickness 5μ , $T = 110^\circ\text{K}$ (\circ), third order of reflection. The curves were calculated under the assumption that the crystal has a mosaic structure.

single-crystal films, and also I. B. Naumov for taking part in the development of the cryostat, and R. S. Silakov, B. I. Barakht'yan, P. F. Samarín, and S. B. Chugunov for help with the experiments.

- ¹V. Weisskopf, *Ann. Phys.* **9**, 23 (1931).
- ²W. Heitler, *The Quantum Theory of Radiation*, Oxford, 1953.
- ³A. Kastler, *Compt. rend.* **250**, 509 (1960).
- ⁴C. Tzara, *J. phys. rad.* **22**, 303 (1961).
- ⁵A. Afanas'ev and Yu. Kagan, *Zh. Eksp. Teor. Fiz.* **48**, 327 (1965) [*Sov. Phys.-JETP* **21**, 215 (1965)]. Yu. Kagan and A. M. Afanas'ev, *ibid.* **49**, 1504 (1965) [**22**, 1032 (1966)].
- ⁶A. M. Afanas'ev and Yu. Kagan, *ZhETF Pis. Red.* **2**, 130 (1965) [*JETP Lett.* **2**, 81 (1965)]. Yu. Kagan and A. M. Afanas'ev, *Zh. Eksp. Teor. Fiz.* **50**, 271 (1966) [*Sov. Phys.-JETP* **23**, 178 (1966)].
- ⁷P. J. Black and J. P. Duerdoth, *Proc. Phys. Soc.* **84**, 169 (1964).
- ⁸P. J. Black and P. B. Moon, *Nature* **188**, 481 (1960); P. J. Black, D. E. Evans, and O'Connor, *Proc. Roy. Soc. A* **270**, 168 (1962).
- ⁹P. J. Black, D. Longworth, and D. A. O'Connor, *Proc. Phys. Soc.* **83**, 925 (1964).
- ¹⁰Yu. Kagan, A. M. Afanas'ev, and I. Perstnev, *Zh. Eksp. Teor. Fiz.* **54**, 1530 (1968) [this issue p.819].
- ¹¹V. K. Voítovetskiĭ, I. L. Korsunskiĭ, and N. S. Tolmacheva, *PTÉ* No. 4, 1968.
- ¹²Mössbauer Effect Data Index (Issue 3), North American Aviation Science Center (1965).
- ¹³K. Siegbahn, *Beta and Gamma Spectroscopy*, North Holland, 1959; C. Hohenemser, *Phys. Rev.* **139**, A185 (1965); H. P. Hanson, F. Herman, J. D. Lea, and S. Skillman, *Acta Cryst.* **17**, 8, 1040 (1964).
- ¹⁴V. K. Voítovetskiĭ, I. L. Korsunskiĭ, A. I. Novikov, and Yu. F. Pazhin, *ZhETF Pis. Red.* **7**, 330 (1968) [*JETP Lett.* **7**, 258 (1968)].

Translated by J. G. Adashko
160